Picosecond transient thermoreflectance for thermal conductivity characterization

Jihoon Jeong, Xianghai Meng, Ann Kathryn Rockwell, Seth R Bank, Wen-Pin Hsieh, Jung-Fu Lin & Yaguo Wang

To cite this article: Jihoon Jeong, Xianghai Meng, Ann Kathryn Rockwell, Seth R Bank, Wen-Pin Hsieh, Jung-Fu Lin & Yaguo Wang (2019): Picosecond transient thermoreflectance for thermal conductivity characterization, Nanoscale and Microscale Thermophysical Engineering

To link to this article: https://doi.org/10.1080/15567265.2019.1580807

Published online: 22 Feb 2019.

Submit your article to this journal

View Crossmark data

Taylor & Francis
Taylor & Francis Group

Check for updates

Picosecond transient thermoreflectance for thermal conductivity characterization

Jihoon Jeong [ORCID][a], Xianghai Meng[a], Ann Kathryn Rockwell[b], Seth R Bank[b], Wen-Pin Hsieh[c], Jung-Fu Lin[d,e], and Yaguo Wang[a,e]

[a]Department of Mechanical Engineering, The University of Texas at Austin, Austin, TX, USA; [b]Department of Electrical and Computer Engineering, The University of Texas at Austin, Austin, TX, USA; [c]Institute of Earth Sciences, Academia Sinica, Nankang, Taipei, Taiwan; [d]Jackson School of Geosciences, The University of Texas at Austin, Austin, TX, USA; [e]Texas Materials Institute, The University of Texas at Austin, Austin, TX, USA

ABSTRACT

We developed a picosecond transient thermoreflectance (ps-TTR) system for thermal property characterization, using a low-repetition-rate picosecond pulsed laser (1064 nm) as the heating source and a 532 nm CW laser as the probe. Low-repetition-rate pump eliminates the complication from thermal accumulation effect. Without the need of a mechanical delay stage, this ps-TTR system can measure the thermal decay curve from 500 ps up to 1 ms. Three groups of samples are tested: bulk crystals (glass, Si, GaAs, and sapphire); MoS_2 thin films (157 ~ 900 nm thickness); InGaAs random alloy and GaAs/InAs digital alloy (short period superlattices). Analysis of the thermoreflectance signals shows that this ps-TTR system is able to measure both thermal conductivity and interface conductance in nanostructures. The measured thermal conductivity values in bulk crystals, MoS_2 thin films, and InGaAs random alloy are all consistent with literature values. Cross-plane thermal conductivity in MoS_2 thin films does not show obvious thickness dependence. Thermal conductivities of GaAs/InAs digital alloys are smaller than InGaAs random alloy, due to the efficient scattering at interfaces. We also discuss the advantages and disadvantages of this newly developed ps-TTR system comparing with the popular time-domain thermoreflectance system.

Introduction

As develping micro-/nano-scale size electronics, thermal management becomes critical due to their higher power density. One fundamental problem of thermal management is the characterization of thermophysical properties. In the past decade, noncontact thermoreflectance techniques have been invented in various forms, such as time-domain thermoreflectance (TDTR) [1], [2], frequency-domain thermoreflectance (FDTR) [3]–[5], transient thermoreflectance (TTR) [6], transient thermal grating [7], [8], and transient grating imaging [9]. Even though different in experimental configurations and analytical models, the common feature of these techniques is the use of a strong pump laser as the heating source to elevate the surface temperature and a weak probe laser to monitor the surface temperature change. TDTR employs a high-repetition-rate laser (e.g. 80 MHz) in conjunction with a pump beam chopped at high frequencies with electro-optic modulator (EOM). The time delay of TDTR is controlled with a mechanical delay stage and signal is acquired with a lock-in amplifier. Experimental signals of TDTR have good sensitivity to thermal conductivities of nanostructures and thermal interface resistance/conductance [2]. Because the duration between pulses is not enough for the

---

CONTACT Yaguo Wang [envelope] yaguo.wang@austin.utexas.edu; Jung-Fu Lin [envelope] afu@jsg.utexas.edu [icon] Texas Materials Institute, The University of Texas at Austin, USA

system to recover its original thermal state [10], the effect of heat accumulation needs to be considered for data analysis. Use of the mechanical delay stage limits the total detection time to less than 20 ns. FDTR technique uses either pulsed lasers or continuous wave (CW) lasers for both pump and probe and measures signal in frequency domain, instead of time domain, over a wide range of modulation frequency. FDTR can measure the thermal conductivity and heat capacity of a sample simultaneously if the thermal diffusivity is larger than 3×10^{-6} m^2/s [3]. However, it also means that it is challenging to investigate low-κ materials using FDTR. Both TDTR and FDTR can also measure in-plane thermal conductivity by carefully varying spot sizes and modulation frequencies [3], [11].

In this work, we developed a picosecond transient thermorefletance system (ps-TTR) that utilizes a low-repetition-rate picosecond laser as pump and a CW laser as probe. This ps-TTR system has several advantages that make it appealing for thermal property characterization. (1) It detects a thermal decay signal excited by a single pulse. The time between pulses is 1 ms, long enough for the sample surface temperature to return to its original state. No heat accumulation effect is expected. (2) Using a CW probe eliminates the need of a mechanical delay stage. The delay time could be as long as 1 ms, only limited by the pump laser repetition rate. (3) Fast data acquisition could be achieved with a digital oscilloscope [6]. (4) The traditional nanosecond TTR (ns-TTR) technique usually utilizes laser pulse with duration of 5 ~ 10 ns, which is not able to detect heat transport in nanostructures. With some iterative fitting procedure, ns-TTR can be sensitive to the interface conductance between metal film and bulk samples [6], but not in nanostructures. This ps-TTR system can measure thermal conductivity in nanostructures as well as interfacial thermal conductance. (5) A grating imaging technique, recently developed in our group [9] and similar to the heterodyned transient grating technique [7], [8], can be incorporated into this ps-TTR system for in-plane thermal conductivity measurement. With this newly developed ps-TTR system, we firstly examine thermal conductivities in four bulk materials, including glass, Si, GaAs, and sapphire, and then tested nanostructures including MoS$_2$ thin-films over a wide range of thicknesses, and digital alloy samples of GaAs/InAs. Finally, we discuss the advantages/disadvantages of this ps-TTR method comparing with the popular TDTR technique.

Experimental

The schematic layout of this ps-TTR system is shown in Figure 1. A picosecond pulsed laser (Coherent Talisker Ultra 532–8, 1064 nm central wavelength, 15 ps pulse width, and 200 kHz repetition rate) is used as the pump and a Nd:YAG laser (532 nm, CW, Coherent Verdi V6) as the
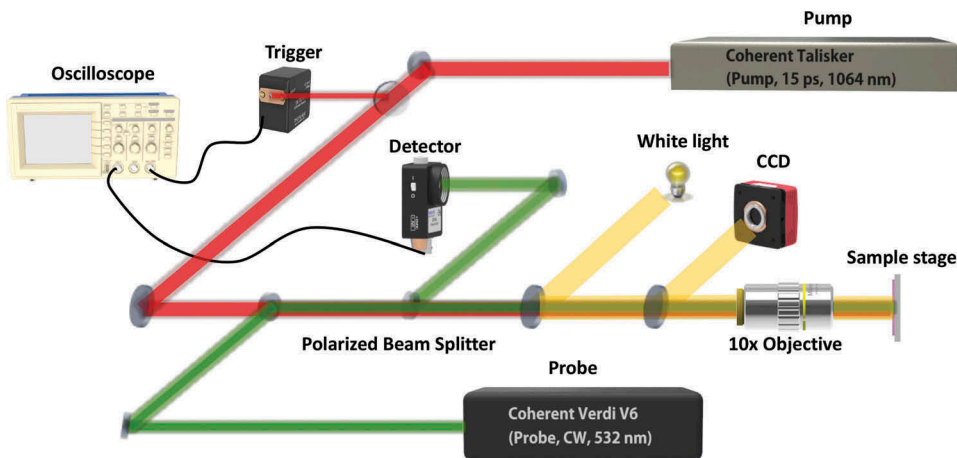

Figure 1. Schematics of ps-TTR set-up.

probe. With an acoustic-optical modulator-based divisor, we further reduce the repetition rate to 1 kHz by picking up one pulse per 200 pulses. A 10× objective lens is used to focus both the pump and probe beams onto the sample surface, and the reflected probe beam is collected by a Hamamatsu C5658 silicon avalanche photodiode with 1 GHz bandwidth (pulse response full width at half maximum, FWHM: 500 ps). The signal traces are recorded on an oscilloscope with 4 GHz bandwidth (Tektronics TDS 744A). Each experimental curve is averaged over more than 10,000 scans and the typical acquisition time is about 5 ~ 10 min. The pump spot diameter ($1/e^2$) is about 125 μm while the probe diameter is about 10 μm. For all the samples measured, the upper limit of thermal penetration depth is less than 11 μm ($d_p = \sqrt{\alpha t_p}$; estimated using the thermal diffusivity of silicon, $\alpha = 9.34 \times 10^{-5}$ m^2/s and the longest fitting time range $t_p = 300$ ns), which is much smaller than the pump spot diameter. These conditions ensure that cross-plane thermal transport is dominant and a simple one-dimensional thermal conduction model can be used to extract the cross-plane thermal conductivity. Metal thin films are deposited onto all sample surfaces as heat transducers to enhance thermoreflectance signal and to maintain a linear relation between reflectance and temperature change. When choosing the metal transducer, preferred are high thermoreflectance coefficient (dR/dT) and low absorbance (1-R) at probe wavelength. High dR/dT value will provide high measurement sensitivity and low absorbance will avoid unnecessary heating from probe laser. Based on these conditions, Au thin film is selected as metal transducer due to its high thermoreflectance value (~ 2×10^{-4} K^{-1}) and low absorbance (<0.3) at probe wavelength (532 nm) [12].

To simulate the experimental results and extract thermal properties, a multi-layer 1D thermal diffusion model, including the metal transducer, sample, and substrate (when applicable), is solved in time domain with Finite Difference Method [6]:

$$\rho_m c_m \left(\frac{\partial T_m}{\partial t} \right) = \frac{\partial}{\partial z} \left(\kappa_m \frac{\partial T_m}{\partial z} \right) + S(z, t) \tag{1}$$

$$\rho_s c_s \left(\frac{\partial T_s}{\partial t} \right) = \frac{\partial}{\partial z} \left(\kappa_s \frac{\partial T_s}{\partial s} \right) \tag{2}$$

where ρ is the density, c is the heat capacity, κ is the thermal conductivity, and S is the source term due to pump laser heating. The subscripts m and s denote the metal transducer and sample, respectively. The source term is only considered in the metal layer. The repetition-rate of our picosecond laser system is set at 1 kHz, which is low enough to guarantee that temperature in the material completely relaxes back to its initial value between pulses. A typical thermal relaxation time in our samples is only several hundred nanoseconds, as shown in Figures 2(a) and 3(c). Therefore, no thermal accumulation effect is considered here. The source term is described as [16] follows:

$$S(z, t) = \frac{0.94 \left(1 - R_{pump} \right) F}{t_p \delta \left[1 - \exp\left(-\frac{L}{\delta} \right) \right]} \exp \left[-2.77 \frac{\left(t - 2t_p \right)^2}{t_p^2} - \frac{z}{\delta} \right] \tag{3}$$

where R_{pump} is the sample reflectivity at the pump laser wavelength, F is the laser fluence, t_p is the pulse width, δ is the optical absorption depth, and L is the thickness of the metal layer. The assumption is that the pump laser energy is only absorbed in the metal layer. We used 50 nm or 80 nm gold as transducer, and the estimated temperature rise under the pump power of 1 mW (pulse energy 1 μJ) is 13 K and 8 K, respectively. (See supplemental material for details.) The absorption depth of Au at 1064 nm is only 12 nm, which validates our assumption. The boundary conditions are given by:
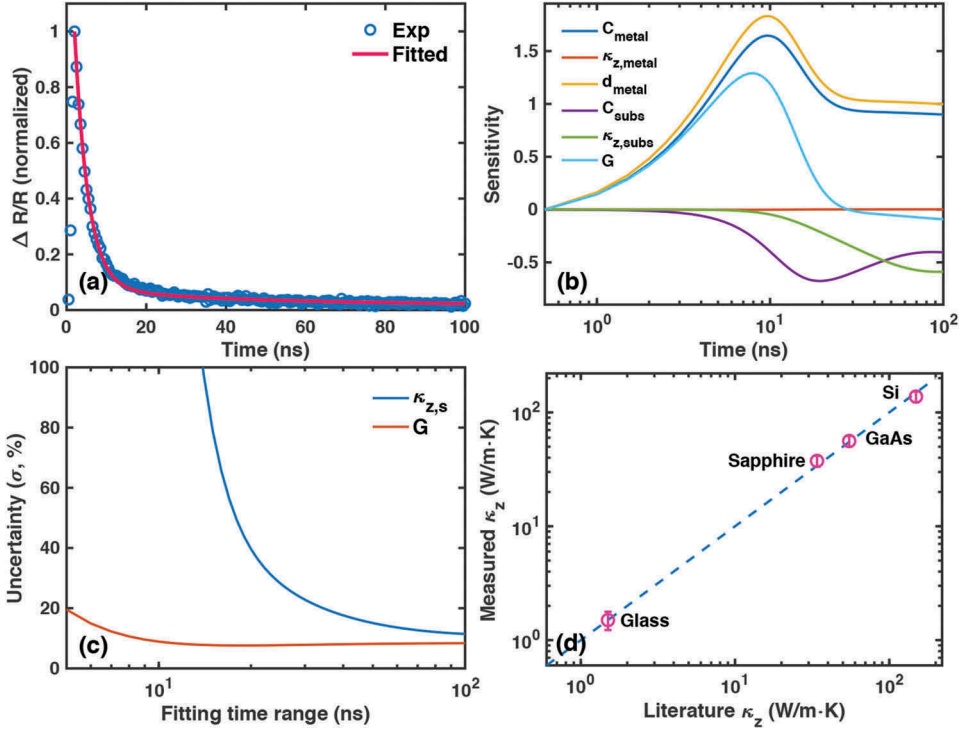
Figure 2. (a) Experimental and fitting results for Au (50 nm) on sapphire. (b) Sensitivity results for all parameters related to the fitting process. (c) Uncertainties of sapphire thermal conductivity and interface resistance based on sensitivity results. (d) Thermal conductivity of glass, sapphire, GaAs, and Si measured with ps-TTR system, along with literature values [13]–[15].

$$-\kappa_m \frac{\partial T_m}{\partial z}\Big|_{z=L} = -\kappa_s \frac{\partial T_s}{\partial z}\Big|_{z=L} = G(T_m - T_s)\big|_{z=L} \tag{4}$$

where G is the interfacial thermal conductance between metal and sample. If another substrate is used, a third layer will be added and Eq. (2) and (4) will be applied to the substrate and sample/substrate interface, respectively.

Results and discussion

In order to validate this ps-TTR system, four bulk materials are measured first, including glass, sapphire, GaAs, and Si. A 50 nm Au thin film is deposited on the sample surface by e-beam evaporator. The Au thin film thickness is determined with profilometer (Dektak 6M Stylus Profilometer). Experimental data and the fitting for sapphire is plotted in Figure 2a. Both the experimental data and the simulated temperature curve are normalized at 500 ps time delay (peak in Figure 2), where the peak experiment value is. After normalization, the experimental curves are independent of pump power and the absolute temperature in Au layer increases with pump power (Figure S3). Several parameters need to be considered for the fitting process, including heat capacity (c), thermal conductivity (κ), and thickness (d) for both Au layer and the sample, as well as the interface conductance (G) between Au and sample. The only unknown parameters are thermal conductivity of the sample and the interface conductance between Au/sample. Reference values are used for all other parameters (listed in Table 1) [17]. Since the delay time of ps-TTR system could be up to 1 ms (due to the repetition rate of 1 kHz), it is important to choose a proper time range for fitting, where the
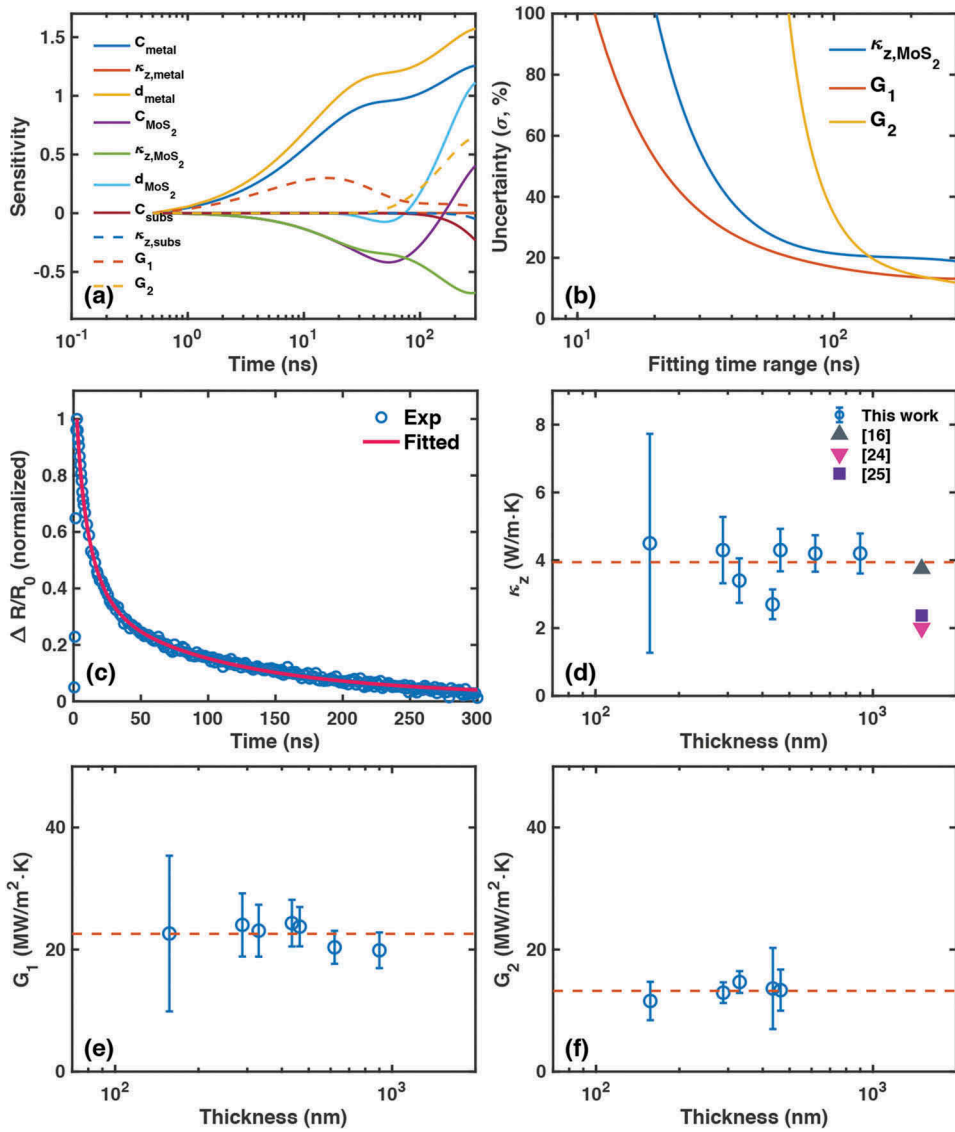
Figure 3. Case study of Au (80 nm) on MoS_2 (464 nm) on SiO_2 (90 nm)/Si substrate. (a) Sensitivity analysis for all parameters related to the fitting process. (b) Uncertainties of MoS_2 thermal conductivity and interface conductance (G_1 and G_2), based on sensitivity results. (c) Experimental and fitting results. Fitted values of (d) κ_{MoS2}, (e) G_1 and (f) G_2 in MoS_2 thin films. For each thickness, five different spots are measured and averaged to calculate the error bars.

Table 1. Thermophysical properties used in simulation model.

	Density (kg/m³)	Heat capacity (J/kg·K)	Thermal conductivity (W/m· K)
Au [17], [18]	19300	129.1	310
Si [14], [15]	2329	710	149
GaAs [14], [15]	5317	350	55
Sapphire [13]	3835	879	34
Glass [19]	2650	700	1.5
MoS_2 [13], [20], [21]	5060	373.5	2 ~ 5

temperature decay curve is most sensitive to the parameters sought. As shown in Figure 2b for sapphire, sensitivity analysis reveals the most sensitive time range for each parameter (See supplemental material for details). The conductance at Au/sapphire interface, G, has the highest sensitivity before 10 ns, whereas thermal conductivity of sapphire is most sensitive around 100 ns. Here, we employ a multi-parameter fitting process to extract κ_s and G. The time range chosen for fitting can affect the extracted thermal conductivity values. To minimize the uncertainty caused by this step, we also conducted the fitting with different time ranges. We found the fitting values of κ_s and G converged when the time range is long enough (Figure S2). Uncertainty analysis for two parameters including κ_s and G is performed using Jacobian matrix between known and unknown parameters [13], [19] [See supplemental material]. Uncertainty values are calculated with 10% uncertainty for d_{metal} and 3% for other parameters, since it is difficult to measure metal film thickness very accurately. As shown in Figure 2c, the resulted uncertainty for both κ ang G reaches its lowest value around 100 ns and becomes almost constant thereafter. The extracted thermal conductivities are plotted in Figure 2d, along with values reported in the literature. The κ_s value is 1.5 ± 0.3 W/m· K for glass, 37 ± 4 W/m· K for sapphire, 56 ± 10 W/m· K for GaAs, and 138 ± 15 W/m· K for Si. The interface conductance G obtained is 48 ± 5 MW/m^2·K for glass, 34 ± 8 MW/m^2·K for sapphire, 22 ± 5 MW/m^2·K for GaAs, and 30 ± 3 MW/m^2·K for Si. The error bars in Figure 2d contain both experimental and fitting uncertainties. Both the measured thermal conductivity [13]–[15] and interface conductance [6], [22–25] are consistent with literature values, which validates our ps-TTR system.

We also utilize this ps-TTR system to measure thermal conductivity in MoS$_2$ thin films, a most studied member in the transition metal dichalcogenides (TMDs) family. MoS$_2$ thin films are prepared via mechanical exfoliation from bulk crystal (purchased from 2Dsemiconductors) and then transferred onto SiO$_2$ (90 nm)/Si substrates using non-residual tape from UltraTape. Seven samples with different thickness are prepared, including 157, 288, 330, 435, 464, 620, and 900 nm, measured with atomic force microscope (Asylum MFP-3D). An 80 nm Au thin film is used as a thermal transducer. The known parameters are the heat capacity (c_{metal}), thermal conductivity (κ_{metal}), and thickness (d_{metal}) of Au layer; heat capacity (c_{MoS2}) and thickness (d_{MoS2}) of MoS$_2$; and heat capacity (c_{subs}) and thermal conductivity (κ_{subs}) of Si substrate, as indicated in Table 1. The three unknown fitting parameters are thermal conductivity of MoS$_2$ (κ_{MoS2}), interfacial thermal conductance (G_1) between Au and MoS$_2$, and interfacial thermal conductance (G_2) between MoS$_2$ and Si substrate. For the fitting process, we consider the 90 nm SiO$_2$ layer as part of the MoS$_2$/Si interface, G_2. We compared the fitting results with that treating the SiO$_2$ as an individual layer and obtained essentially the same values because the temperature decay curve is not sensitive to SiO$_2$ heat capacity (Figure S8). Several steps are taken to obtain accurate fitting values: (1) perform sensitivity test for all parameters to find the most sensitive time range for each unknown parameter; (2) calculate uncertainty for κ_{MoS2}, G_1, and G_2 based on the sensitivity results; and (3) select a fitting time range where κ_{MoS_2} is most sensitive with minimized uncertainty. Figure 3 demonstrates the case of a 464 nm MoS$_2$ thin film. Figure 3a shows an example of sensitivity results and, Figure 3b gives uncertainties for κ_{MoS_2}, G_1, and G_2. Uncertainty values are calculated with 10% uncertainty for d_{metal}, and 3% for other parameters. As shown in Figure 3a, sensitivity for G_1 shows a peak before 20 ns and while κ_{MoS2} is most sensitive at around 300 ns time range. This is also the time when uncertainty for κ_{MoS2} is minimized, as shown in Figure 3b. Therefore, the fitting time range is selected to be 300 ns since our most interested parameter is κ_{MoS2}. One example of experimental data and the fitting is presented in Figure 3c. Figure 3d~3f shows the fitted values of κ_{MoS2}, G_1, and G_2. For the 620 and 900 nm samples, G_2 values are not displayed, because in thick samples the experimental data is not sensitive to G_2. All results do not show an obvious trend with MoS$_2$ thickness, and the averaged values are κ_{MoS2} = 3.9 ± 0.2 W/m· K, G_1= 22.5 ± 0.7 MW/m^2·K, and G_2= 13.2 ± 0.5 MW/m^2·K. The error bars include both experimental and fitting uncertainty. The average thermal conductivity value is within the range of previously reported values as 4.75 ± 0.32 W/m· K [13], 2.0 ± 0.2 W/m· K [20], and 2.37 W/m· K [21]. First-principle calculations in Van der Waals' solids suggest that strong thickness-dependent cross-plane thermal conductivity is only expected when phonon mean free path (MFP) is comparable with sample thickness, where boundary scattering dominates over phonon–

phonon scattering [26]. So far, there is no experimental investigation of thickness-dependent cross-plane thermal conductivity in MoS_2. Thickness dependence of in-plane thermal conductivity is reported in MoS_2 less than 10 layer thick [27]. There have been many calculations about basal-plane MFP in monolayer MoS_2, with a range of 10–40 nm [28]–[31]. Usually, the cross-plane phonon MFP is much shorter than the in-plane one, and hence much shorter than the thickness of all our MoS_2 thin films. This explains why no thickness dependence is observed. Using fs-TDTR technique, modulation-frequency-dependent cross-plane thermal conductivity has been reported in bulk MoS_2, which was explained by different thermal penetration depth varying with modulation frequency [13]. However, according to a recent publication, the modulation-frequency-dependent thermal conductivity observed in TMDs could also be due to non-equilibrium thermal resistance between high-frequency optical phonons and acoustic phonons in TMDs [13]. In our measurement, the separation time between pump pulses is 1 ms. From Figure 3c, the sample surface temperature has already returned to its ambient state after 300 ns, which means all the phonons have reached an equilibrium state at ambient temperature. Therefore, the measured thermal conductivities using this ps-TTR technique are simply intrinsic values. In WS_2, Lindroth et al. predicted a much longer MFP, 686 nm along the in-plane direction (this value is 10× more than others' results [28]–[31]) and 239 nm along the out-of-plane direction. A clear thickness dependence was observed in both WS_2 and MoS_2, even beyond 1 μm thickness [26]. Using our measured cross-plane thermal conductivity of MoS_2 (~4 W/m· K) and a characteristic decay time about 100 ns (~10% of peak value), the penetration depth in MoS_2 is estimated as about 450 nm. If there is indeed a thickness dependence, it should be more prominent in thinner samples, which was not observed in our experiments. Therefore, our thickness-dependent measurements suggest a much smaller cross-plane phonon MFP in MoS_2 than the value predicted by Lindroth.

Mao et al. predicted the interfacial thermal resistance between metal and MoS_2 with first-principle calculations based on the Landauer formalism [32]. The calculated value for Au/MoS_2 interface resistance is 58 m^2·K/GW, which is equal to an interface conductance of 17.2 MW/m^2·K. Jiang et al. reported modulation-frequency-dependent G_1 value between Al and MoS_2, and the G_1 value at the lowest modulation frequency of 0.7 MHz is around 35 MW/m^2·K [13]. For Au on graphite, Schmidt et al. reported an interface conductance value of ~35 MW/m^2·K [33]. Our measured G_1 values are consistent with these literature values.

The third group of samples tested are alloys, with the information listed in Table 2. The actual sample structure is demonstrated in Figure 4a. All the samples are grown by solid-source molecular beam epitaxy, lattice matched on semi-insulating InP substrates [34]. Alloy #1 is a conventional random alloy, $In_{0.53}Ga_{0.47}As$, where the Ga, In, and As shutters are all open simultaneously, and the composition is controlled by the source temperature. Alloy #2 & #3 are digital alloys, consisting of periodic layers of GaAs and InAs, where the composition is controlled by the duty of cycle of the shutter as opposed to source temperature. The period thickness of these digital alloy is 2.35 nm (3.76 monolayer (ML) GaAs/4.24 ML InAs per period), and 107 periods in total. While some digital alloys have been shown to possess properties beneficial for photodetectors [35], the thermal properties of

Table 2. Sample information on InGaAs digital and random alloys.

	Alloy #1	Alloy #2	Alloy #3
Type	Random alloy ($In_{0.53}Ga_{0.47}As$)	Digital alloy (GaAs/InAs)	Digital alloy (GaAs/InAs)
Alloy thickness	250 nm	250 nm	250 nm
Period thickness	N/A	2.35 nm[a]	2.35 nm[a]
Cap layer	N/A	10 nm InGaAs	N/A
Buffer layer	N/A	100 nm InGaAs	200 nm InGaAs

a One ML GaAs has a thickness of 0.2827 nm, one ML InAs has a thickness of 0.3029 nm, and one ML InGaAs has a thickness of 0.2934 nm·
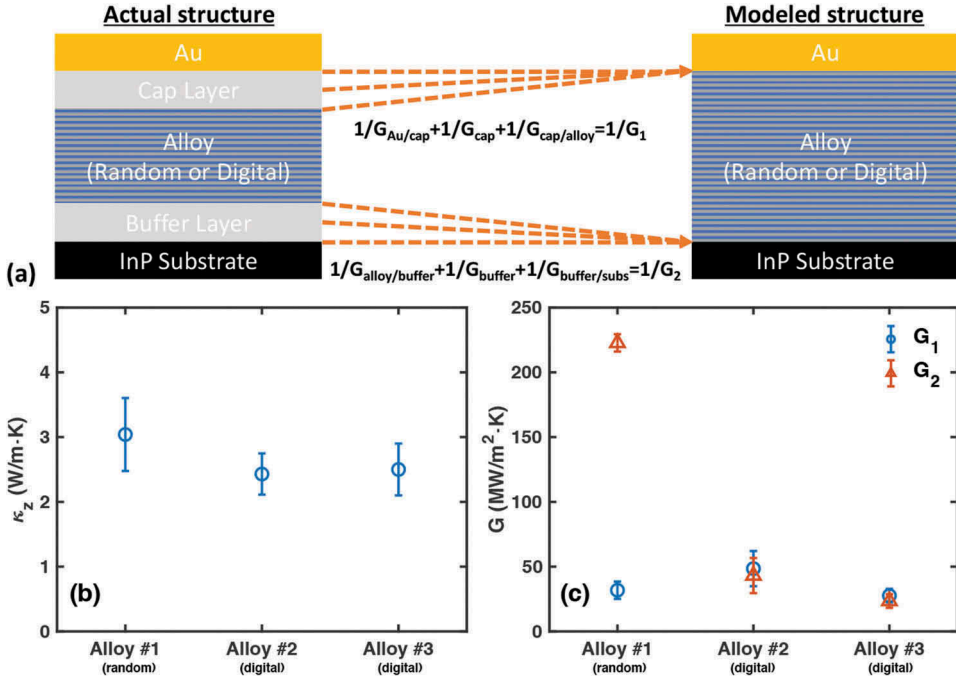
Figure 4. (a) Schematic diagram of the actual sample structure (left) and modeled structure for fitting (right). Results of three different alloy samples: (b) thermal conductivity, (c) the first and second interface thermal conductance (G_1 & G_2).

these alloys remain largely unknown. For alloy #2 & #3, an InGaAs buffer layer is firstly grown on the substrate to smoothen and prime the surface for high-quality growth of the active layers. Alloy #2 also has a cap layer to prevent oxidation of the sample surface after growth.

For thermal conductivity measurement, we deposited a 50 nm Au thin film on all samples. For numerical simulation, we only consider three layers, Au film, alloy, and substrate, as shown in Figure 4a. Effects from cap layer and buffer layer are lumped into two interface conductance (G_1 and G_2). Treating the thick buffer layer as part of the second interface may seem unjustified, especially when the temperature decay curve is sensitive to both the heat capacity and thermal conductivity of buffer layer (Figure S7). The InGaAs buffer layer was used to compensate the lattice mismatch between digital alloy and InP substrate and hence reduce the stress in digital alloy. The interface conductance between digital alloy and InGaAs buffer is expected to be large. Assuming an interface conductance of 100 MW/m²·K and a thermal conductivity of 3 W/mK for InGaAs buffer, the Kapitza length is estimated to be only about 3 nm. Since the buffer layer thickness is 100 nm for digital alloy #2 and 200 nm for digital alloy #3, the temperature decay curve has almost negligible sensitivity to the alloy/buffer interface (Figure S6 & S7). Therefore, treating the buffer layer as an individual layer is not feasible in this case. For alloy layer, the values averaged over GaAs and InAs by their weight ratio (47:53) are used for heat capacity (297 J/kg·K) and density (5504 kg/m³), given that for GaAs ρ = 5317.6 kg/m³, c = 350 J/kg·K, and for InAs ρ = 5670 kg/m³, c = 250 J/kg·K.

Obtained thermal conductivities from fitting are 3.0 ± 0.6 W/m· K for alloy #1, 2.4 ± 0.3 W/m· K for alloy #2, and 2.5 ± 0.4 W/m· K for Alloy #3, as plotted in Figure 4b. Since reported thermal conductivity value of bulk $In_{0.5}Ga_{0.5}As$ (random alloy) is about 5 W/m· K [36], [37], our measured value for the random alloy is relatively low (3.0 ± 0.6 W/m· K). Considering the thickness of 250 nm, the value measured here can be explained by the thickness-dependent thermal conductivity when the film thickness is shorter than phonon MFP. Koh et al. has reported modulation frequency (f)–dependent thermal conductivity in InGaAs alloy [38], where the modulation frequency determines the thermal

penetration depth by a relation of $d_p = \sqrt{\kappa/\pi f \rho c}$. When the thermal penetration depth is shorter than the phonon MFP, ballistic thermal transport starts to play a role, and the measured thermal conductivity is lower than the intrinsic value of bulk. According to reported accumulated thermal conductivities, phonon MFP of GaAs and InAs is on the order of hundreds of nanometers [39], [40], which is comparable with the thickness of our random alloy. So ballistic heat transport could play a role in our measured thermal conductivity. With thermal penetration depth about 250 nm, the measured thermal conductivity value deduced from [38] is in the range of 3 ~ 4 W/m· K, which is consistent with our results (3.0 ± 0.6 W/m· K). Digital alloys (#2 & #3) have lower thermal conductivities, which is a result of very effective phonon scattering at interfaces. Similar phenomena have been observed in previous publications [41]–[43]. Thermal conductance across two interfaces (G_1 for Au/Alloy interface and G_2 for Alloy/substrate interface) are plotted in Figure 4c. Alloy #3 has the smallest G_2 value, which is reasonable because it has the thickest buffer layer.

By characterizing three groups of samples, we have shown that this newly developed ps-TTR system can measure both thermal conductivity and interface resistance with good accuracy. Lastly, we want to comment on the differences between this ps-TTR system and the popular TDTR system. As regard to the experimental set-up, ps-TTR uses a low-repetition-rate pump laser, a CW probe laser and a fast photodiode working with an oscilloscope for data acquisition. For TDTR, both pump and probe are pulses from a high-repetition-rate laser. Time delay between pump and probe is controlled with mechanical delay stage. EOM working with a lock-in amplifier is used for data acquisition. EOM modulation allows control of thermal penetration depth by tuning the modulation frequency. The tunable modulation frequency of TDTR provides an extra free parameter and is useful for many purposes, for example, the phonon MFP spectroscopy. The experimental setup of ps-TTR is much simpler and cost-effective. For example, a 1064 nm laser with ~400 ps pulse width can cost as low as $12K (RMPC, Wedge-XF-1064), which is even cheaper than a long-range mechanical delay stage. Both systems can be modified to measure in-plane thermal conductivity as well. For TDTR, techniques such as offset laser beams [44] and varying pump or probe laser spot size [11] have been implemented. For ps-TDTR, our recently developed grating imaging technique [9], [45] can be integrated with ease. As regard to the thermal model to extract thermal properties from experimental data, for ps-TDTR we use the finite difference method to solve a simple thermal diffusion model numerically. For FDTR, the thermal diffusion model considers the heat accumulation effect and is usually solved in frequency domain analytically. Even though numerical simulation is more expensive computationally, it provides a great amount of flexibly to consider effects from laser penetration depth at different wavelengths, pulse duration, pulse shape, etc. TDTR was reported to be sensitive to thermal effusivity ($e = \sqrt{\kappa \rho c_p}$) at a high modulation frequency and to thermal diffusivity ($\alpha = \kappa/\rho c_p$) at a low modulation frequency [46], [47]. Our ps-TTR system is mainly sensitive to thermal effusivity. The detector in our current ps-TTR system has a time resolution of 500 ps, which is the limiting factor for measuring thermal conductivity in films much thinner than 100 nm.

Conclusion

We developed a ps-TTR technique for thermal property characterization. This system provides a time delay up to 1 ms, only limited by the laser repetition rate, as well as a time resolution of 500 ps, limited by the photodetector response time. The measured thermal conductivity values in bulk crystals, MoS_2 thin films, and InGaAs random alloy are all consistent with literature values. Our analysis has shown that experimental data taken with this ps-TTR system is sensitive to both thermal conductivity and interface conductance in nanostructures.

Acknowledgments

ORCID

Jihoon Jeong Ⅾ http://orcid.org/0000-0002-2427-8010

References

[1] C. A. Paddock and G. L. Eesley, "Transient thermoreflectance from thin metal films," *J. Appl. Phys.*, vol. 60, no. 1, pp. 285–290, Jul. 1986. DOI: 10.1063/1.337642.

[2] D. G. Cahill, "Analysis of heat flow in layered structures for time-domain thermoreflectance," *Rev. Sci. Instrum.*, vol. 75, no. 12, pp. 5119–5122, Dec. 2004. DOI: 10.1063/1.1819431.

[3] A. J. Schmidt, R. Cheaito, and M. Chiesa, "A frequency-domain thermoreflectance method for the characterization of thermal properties," *Rev. Sci. Instrum.*, vol. 80, no. 9, pp. 094901–6, Sep. 2009. DOI: 10.1063/1.3212673.

[4] A. J. Schmidt, R. Cheaito, and M. Chiesa, "Characterization of thin metal films via frequency-domain thermoreflectance," *J. Appl. Phys.*, vol. 107, no. 2, pp. 024908–6, Jan. 2010. DOI: 10.1063/1.3289907.

[5] K. T. Regner, *et al.* "Broadband phonon mean free path contributions to thermal conductivity measured using frequency domain thermoreflectance," *Nat. Commun.*, vol. 4. pp. 1640–1647, Mar. 2013. DOI:10.1038/ncomms2630.

[6] R. Garrelts, A. Marconnet, and X. Xu, "Assessment of thermal properties via nanosecond thermoreflectance method," *Nanosc. Microsc. Therm. Eng.*, vol. 19, no. 4, pp. 245–257, Dec. 2015. DOI: 10.1080/15567265.2015.1078425.

[7] O. W. Kading, H. Skurk, A. A. Maznev, and E. Matthias, "Transient thermal gratings at surfaces for thermal characterization of bulk materials and thin films," *Appl. Phys. A.*, vol. 61, pp. 253–261, Apr. 1995. DOI: 10.1007/BF01538190.

[8] A. A. Maznev, J. A. Rogers, and K. A. Nelson, "Optical heterodyne detection of laser-induced gratings," *Opt. Lett.*, vol. 23, no. 16, pp. 1319–1321, Aug. 1998. DOI: 10.1364/OL.23.001319.

[9] J. Jeong, *et al.* "In-plane thermal conductivity measurement with nanosecond grating imaging technique," *Nanosc. Microsc. Therm. Eng.*, vol. 22, no. 2, 83–96. Feb. 2018. DOI: 10.1080/15567265.2017.1416713.

[10] W. S. Capinski and H. J. Maris, "Improved apparatus for picosecond pump-and-probe optical measurements," *Rev. Sci. Instrum.*, vol. 67, no. 8, pp. 2720–2726, Aug. 1996. DOI: 10.1063/1.1147100.

[11] P. Jiang, X. Qian, and R. Yang, "Time-domain thermoreflectance (TDTR) measurements of anisotropic thermal conductivity using a variable spot size approach," *Rev. Sci. Instrum.*, vol. 88, no. 7, pp. 074901–9, Jul. 2017. DOI: 10.1063/1.4991715.

[12] R. B. Wilson, B. A. Apgar, L. W. Martin, and D. G. Cahill, "Thermoreflectance of metal transducers for optical pump-probe studies of thermal properties," *Opt. Express*, vol. 20, no. 27, pp.28829–10, 2012. DOI: 10.1364/OE.20.028829.

[13] P. Jiang, X. Qian, X. Gu, and R. Yang, "Probing anisotropic thermal conductivity of transition metal dichalcogenides MX 2(M = Mo, W and X = S, Se) using time-domain thermoreflectance," *Adv. Mater.*, vol. 29, no. 36, pp. 1701068–7, Jul. 2017. DOI: 10.1002/adma.201700681.

[14] K. K. Ng, *Complete Guide to Semiconductor Devices*, New York, John Wiley & Sons, Inc.,1995.

[15] S. M. Sze and K. K. Ng, *Physics of Semiconductor Devices*. Hoboken, NJ, USA: John Wiley & Sons, Inc., 2006.

[16] L. Guo, S. L. Hodson, T. S. Fisher, and X. Xu, "Heat transfer across metal-dielectric interfaces during ultrafast-laser heating," *J. Heat Transfer*, vol. 134, no. 4, pp. 042402, Apr. 2012. DOI: 10.1115/1.4005255.

[17] Y. S. Touloukian, R. W. Powell, C. Y. Ho, and P. G. Klemens. Thermophysical properties of matter - The TPRC data series. *Therm. Conductivity - Metall. Ele. Alloys*, vol. 1, pp. 132 Jan. 1970.

[18] Y. S. Touloukian and E. H. Buyco. Thermophysical properties of matter - The TPRC data series. *Specific Heat - Metall. Ele. Alloys*, vol. 4, pp. 83, Jan. 1971.

[19] J. Yang, E. Ziade, and A. J. Schmidt, "Uncertainty analysis of thermoreflectance measurements," *Rev. Sci. Instrum.*, vol. 87, no. 1, pp. 014901–014912, Jan. 2016. DOI: 10.1063/1.4962023.

[20] J. Liu, G.-M. Choi, and D. G. Cahill, "Measurement of the anisotropic thermal conductivity of molybdenum disulfide by the time-resolved magneto-optic Kerr effect," *J. Appl. Phys.*, vol. 116, no. 23, pp. 233107, Dec. 2014. DOI: 10.1063/1.4904513.

[21] C. Muratore, *et al*. "Cross-plane thermal properties of transition metal dichalcogenides," *Appl. Phys. Lett.*, vol. 102, no. 8, pp. 081604, 2013. DOI: 10.1063/1.4793203.

[22] A. N. Smith, J. L. Hostetler, and P. M. Norris, "Thermal boundary resistance measurements using a transient thermoreflectance technique," *Microsc. Therm. Eng.*, vol. 4, no. 1, pp. 51–60, Oct 2010.

[23] E. Bozorg-Grayeli, J. P. Reifenberg, M. A. Panzer, J. A. Rowlette, and K. E. Goodson, "Temperature-dependent thermal properties of phase-change memory electrode materials," *IEEE Electron Device Lett.*, vol. 32, no. 9, pp. 1281–1283, Aug. 2011. DOI: 10.1109/LED.2011.2158796.

[24] R. J. Stevens, A. N. Smith, and P. M. Norris, "Measurement of thermal boundary conductance of a series of metal-dielectric interfaces by the transient thermoreflectance technique," *J. Heat Transfer*, vol. 127, no. 3, pp.315–318, 2005. DOI: 10.1115/1.1857944.

[25] R. J. Stoner and H. J. Maris, "Kapitza conductance and heat flow between solids at temperatures from 50 to 300 K," *Phys. Rev. B*, vol. 48, no. 22, pp. 16373–15, Dec. 1993. DOI: 10.1103/PhysRevB.48.16373.

[26] D. O. Lindroth and P. Erhart, "Thermal transport in van der Waals solids from first-principles calculations," *Phys. Rev. B*, vol. 94, no. 11, pp. 1060–11, Sep. 2016. DOI: 10.1103/PhysRevB.94.115205.

[27] X. Gu, B. Li, and R. Yang, "Layer thickness-dependent phonon properties and thermal conductivity of MoS 2," *J. Appl. Phys.*, vol. 119, no. 8, pp. 085106, Feb. 2016. DOI: 10.1063/1.4942827.

[28] W. Li, J. Carrete, and N. Mingo, "Thermal conductivity and phonon linewidths of monolayer MoS_2 from first principles," *Appl. Phys. Lett.*, vol. 103, no. 25, pp. 253103, Dec. 2013. DOI: 10.1063/1.4850995.

[29] Y. Cai, J. Lan, G. Zhang, and Y.-W. Zhang, "Lattice vibrational modes and phonon thermal conductivity of monolayer MoS2," *Phys. Rev. B.*, vol. 89, pp. 035438, Jan 2014. DOI: 10.1103/PhysRevB.89.035438.

[30] X. Wei, *et al*. "Phonon thermal conductivity of monolayer MoS2: a comparison with single layer graphene," *Appl. Phys. Lett.*, vol. 105, no. 10, 103902.Sep. 2014. DOI: 10.1063/1.4895344.

[31] J. Su, Z.-T. Liu, L.-P. Feng, and N. Li, "Effect of temperature on thermal properties of monolayer MoS2 sheet," *J. Alloys. Compd.*, vol. 622, pp. 777–782, 2015. DOI: 10.1016/j.jallcom.2014.10.191.

[32] R. Mao, B. D. Kong, and K. W. Kim, "Thermal transport properties of metal/MoS 2interfaces from first principles," *J. Appl. Phys.*, vol. 116, no. 3, pp. 034302, Jul. 2014. DOI: 10.1063/1.4890347.

[33] A. J. Schmidt, K. C. Collins, A. J. Minnich, and G. Chen, "Thermal conductance and phonon transmissivity of metal–graphite interfaces," *J. Appl. Phys.*, vol. 107, no. 10, pp. 104907–6, May. 2010. DOI: 10.1063/1.3428464.

[34] S. J. Maddox, S. D. March, and S. R. Bank, "Broadly tunable aIInAsSb digital alloys grown on GaSb," *Cryst. Growth Des.*, vol. 16, no. 7, pp. 3582–3586, May. 2016. DOI: 10.1021/acs.cgd.5b01515.

[35] M. E. Woodson, *et al*., "Low-noise AlInAsSb avalanche photodiode," *Appl. Phys. Lett.*, vol. 108, no. 8, pp. 081102, Feb. 2016. DOI: 10.1063/1.4942372.

[36] M. S. Abrahams, R. Braunstein, and F. D. Rosi, "Thermal, electrical and optical properties of (In,Ga)as alloys," *J. Phys. Chem. Solid.*, vol. 10, no. 2, pp.204–210, 1959. DOI: 10.1016/0022-3697(59)90076-9.

[37] F. Szmulowicz, F. L. Madarasz, P. G. Klemens, and J. Diller, "Calculation of the lattice thermal conductivity in GaAs-InAs alloys and comparison with experiment," *J. Appl. Phys.*, vol. 66, no. 1, pp. 252–255, Jul. 1989. DOI: 10.1063/1.343865.

[38] Y. K. Koh and D. G. Cahill, "Frequency dependence of the thermal conductivity of semiconductor alloys," *Phys. Rev. B*, vol. 76, no. 7, pp. 075207–5, Aug. 2007. DOI: 10.1103/PhysRevB.76.075207.

[39] T. L. A. J. G. A. J. S. A. K. E. A. G. Chen, "Gallium arsenide thermal conductivity and optical phonon relaxation times from first-principles calculations," *EPL (Europhysics Letters)*, vol. 101, no. 1, pp.16001, 2013. DOI: 10.1209/0295-5075/101/16001.

[40] F. Zhou, *et al*. "Thermal conductivity of indium arsenide nanowires with wurtzite and zinc blende phases," *Phys. Rev. B.*, vol. 83, no. 20, pp. 205416, EP, May, 2011. DOI: 10.1103/PhysRevB.83.205416.

[41] G. Chen, "Thermal conductivity and ballistic-phonon transport in the cross-plane direction of superlattices," *Phys. Rev. B*, vol. 57, no. 23, pp. 14958–16, Jun. 1998. DOI: 10.1103/PhysRevB.57.14958.

[42] F. He, W. Wu, and Y. Wang, "Direct measurement of coherent thermal phonons in Bi2Te3/Sb2Te3 superlattice," *Appl. Phys. A*, vol. 122, no. 8, pp.777, 2016. DOI: 10.1007/s00339-016-0309-z.

[43] R. Venkatasubramanian, "Lattice thermal conductivity reduction and phonon localizationlike behavior in superlattice structures," *Phys. Rev. B*, vol. 61, no. 4, pp. 3091–3097, Jan. 2000. DOI: 10.1103/PhysRevB.61.3091.

[44] J. P. Feser and D. G. Cahill, "Probing anisotropic heat transport using time-domain thermoreflectance with offset laser spots," *Rev. Sci. Instrum.*, vol. 83, no. 10, pp. 104901, Oct. 2012. DOI: 10.1063/1.4757863.

[45] K. Chen, *et al*., "Comparison between grating imaging and transient grating techniques on measuring carrier diffusion in semiconductor," *Nanosc. Microsc. Therm. Eng.*, vol. 22, no. 4, pp. 348–359, Aug. 2018.

[46] J. Liu, *et al*., "Simultaneous measurement of thermal conductivity and heat capacity of bulk and thin film materials using frequency-dependent transient thermoreflectance method," *Rev. Sci. Instrum.*, vol. 84, no. 3, pp. 034902–13, Mar. 2013. DOI: 10.1063/1.4797479.

[47] C. Wei, X. Zheng, D. G. Cahill, and J.-C. Zhao, "Invited article: micron resolution spatially resolved measurement of heat capacity using dual-frequency time-domain thermoreflectance," *Rev. Sci. Instrum.*, vol. 84, no. 7, pp. 071301, Jul. 2013. DOI: 10.1063/1.4815867.